Biosensors and Bioelectronics 137 (2019) 279–286

Contents lists available at ScienceDirect

Biosensors and Bioelectronics

journal homepage: www.elsevier.com/locate/bios

Highly sensitive aptasensor based on interferometric reflectance spectroscopy for the determination of amyloid β as an Alzheimer's disease biomarkers using nanoporous anodic alumina

Mahmoud Amouzadeh Tabrizi, Josep Ferré-Borrull, Lluis F. Marsal*

Departamento de Ingeniería Electrónica, Eléctrica y Automática, Universitat Rovira i Virgili, Avda. Països Catalans 26, 43007 Tarragona, Spain

ARTICLE INFO

Keywords:
Alzheimer's disease
Amyloid β oligomers
Nanoporous anodic alumina
Interferometric reflectance spectroscopy
Aptasensor

ABSTRACT

It is well known that Alzheimer's disease is one of the global challenges for the 21st century. Therefore, it is urgent to develop a reliable biosensor for the detection of this disease. Here in, we have developed for the first time, an aptasensor based on interferometric reflectance spectroscopy (IRS) for the determination of amyloid β (Aβ) oligomers that is an Alzheimer's disease biomarker. For this purpose, the nanoporous anodic alumina (NAA) was first fabricated. After that, the pore walls of the NAA were modified with (3-aminopropyl) trimethoxysilane (NAA-NH_2). The amino-terminal aptamers probe were then attached to the pore walls of the NAA-NH_2 by using glutaraldehyde (GA) as the cross-linking agent. Subsequently, methylene blue (MB) was immobilized into the aptamer as the photo-probe, generating the MB/G-quadruplex complex. Since MB has a high absorption coefficient, the intensity of the reflected white light to the charge-coupled device (CCD) detector decreased. In the presence of the Aβ oligomers that have high affinity to the immobilized aptamer, the MB/quadruplex complex broke and MB washed away from the aptasensor. Therefore, the intensity of the reflected white light to the CCD detector increased. The increased signal intensity of the aptasensor has a logarithmic relationship with the concentration of Aβ oligomers. The proposed aptasensor exhibited a good response to the concentration of Aβ oligomers in the range of 0.5–50.0 μg × mL^{-1}. The experimental detection limit was of 0.02 μg × mL^{-1} (at 3σ/S). The proposed optical aptasensor exhibited good selectivity, linear range, and stability.

1. Introduction

Alzheimer's disease (AD) that a neurodegenerative disorder is the most common type of dementia. There was an estimated the AD will affect115 million people by 2050 in all of the world (eurekalert. 2017). Since no effective cure for the AD has been reported yet, the fabrication of fast and simple analytical device for the determination of biomarker related to the AD such as amyloid β (Aβ) oligomers in the patient fluids such as blood and cerebrospinal fluid is demanded. Aβ that has 42 amino acids in length (Aβ1–42) aggregates in the AD brain (Citron et al., 1996). During this process, Aβ oligomers, then fibrils, and finally plaques are generated, respectively and accumulated in cerebrospinal fluid (Salvadores et al., 2014). However, Aβ oligomers are the most neurotoxic form of Aβ. Because in comparison with Aβ fibrils, the Aβ oligomers have more diffusible (Lublin and Gandy, 2010). It leads to an increase in the number of toxic β-sheets per total mass of Aβ (Tew et al., 2008). Therefore, because of the public health, the fabrication of a highly sensitive sensor for the detection of Aβ is necessary. For this purpose, various bio-receptors have been used to determine Aβ such as antibody (Veloso et al., 2014; Yi et al., 2016; Zhou et al., 2016), cellular prion protein (PrPC) (Rushworth et al., 2014), PrP (95–110) peptide (Liu et al., 2015) and aptamer (Deng et al., 2018; Ke et al., 2018; Zhou et al., 2018). Among them, aptamer-based biosensors (aptasensors) are the most favorited bio-sensing device to diagnose the biomaterials because of the high price of extraction of bio-receptors samples such as antibodies from the biological sample, simple access to the artificial aptamer with different functional groups such as carboxylic acid (Fan et al., 2016), primary amine (Amouzadeh Tabrizi and Shamsipur, 2015), acetylene (Galán et al., 2015) and phosphate (Zhang et al., 2011), biotin (Wu et al., 2010), and thiol (Zarei et al., 2018) and high sensitivity. In addition, aptamer can interact with dye molecules such as methylene blue (Jarczewska et al., 2018; Wang et al., 2009), malachite green (Kolpashchikov, 2005), syber green (SG) (Mc Keague et al., 2014) and berberine (Song et al., 2018), generating the label-free aptasensor to detect the various analytes. Among them, MB not only has a high absorption coefficient (ε = 95000 L × mol^{-1} × cm^{-1}) (Miloševic

* Corresponding author.
E-mail address: lluis.marsal@urv.cat (L.F. Marsal).

https://doi.org/10.1016/j.bios.2019.04.050
Received 15 February 2019; Received in revised form 8 April 2019; Accepted 23 April 2019
Available online 30 April 2019
0956-5663/ © 2019 Elsevier B.V. All rights reserved.

et al., 2013) but also has a specific interaction with guanine-rich aptamer strands (Shamsipur et al., 2015; Zhang et al., 2014). The guanine-rich aptamers strands can self-assemble into the higher ordered structures that named intermolecular G-quadruplex structures (tetra molecular parallel and bimolecular G-quadruplex structures) (Burge et al., 2006; Cao et al., 2017; Song and Ren, 2010). These G-quadruplex structures that are made around four hydrogen-bonded guanines can bind to MB, immobilizing this photo-probe on the biosensor (Shamsipur et al., 2015; Zhang et al., 2014). Up to now, various biosensors have been fabricated for the determination of the biomarkers (Amouzadeh Tabrizi et al., 2018; Bandodkar et al., 2015; Gonçalves et al., 2016). Among them, the contactless biosensors are more interested because of their ability to remote sensing of biomarkers. The light reflectance spectroscopy based biosensors such as optical fiber (Marazuela and Moreno-Bondi, 2002), photonic crystals (Heeres and Hergenrother, 2011), optical resonators (Malmir et al., 2016) and interferometric reflectance spectroscopy (IRS) (Chiavaioli et al., 2017; Rajeev et al., 2018; Stavra et al., 2018) are the four major types of contactless sensors. Among them, the IRS based biosensors are the cheap, highly sensitive and uncomplicated device for the determination of biomaterials (Ferré-Borrull et al., 2014; Kumeria et al., 2014; Mariani et al., 2016). The IRS is one of the optical sensors which is based on white light interference at thin nano/microporous film surfaces such as porous silicon (pSi) (Lin et al., 1997) and NAA (Nemati et al., 2018; ; Santos et al., 2011a,b; Vojkuvka et al., 2008). In this sensor, beams of the white light is directed on the nano/microporous film surfaces. The partial beams of the white light are reflected at each phase boundary finally is detected by using a detector. The interaction of the immobilized receptor with target will change the properties of the reflected light to the detector.

To the best of our knowledge, an aptasensor based IRS for the determination of Aβ oligomers has not been reported yet. To fabricate the aptasensor, the aptamer/MB was immobilized on the pore walls of NAA. This aptamer probe that is considered as the guanine-rich aptamer can interact with MB, generating MB/G-quadruplex complex. In the presence of Aβ oligomers, this complex broke down and MB washed away by phosphate buffer (PB). This change in the structure of the aptasensor changed its optical property. On the basis of these great advantages, the designed IRS based aptasensor exhibited high analytical performance to Aβ oligomers in terms of sensitivity, stability, selectivity, linear range (LR) and limit of detection (LOD).

2. Experimental section

2.1. Reagents and chemicals

All chemicals were of analytical reagent grade and used without further purification. Double deionized (DI) water (18.6 MΩ) was used throughout. Aluminium (Al) discs of 15 mm diameter were obtained from Goodfellow. 3-aminopropyl trimethoxysilane (3-APES), 1,1,1,3,3,3-hexafluoro-2-propanol (HFIP), bovine serum albumin (BSA), oxalic acid (Ox), glutaraldehyde (GLA), methylene blue (MB), phosphoric acid (H_3PO_4), chromium (VI) oxide (H_2CrO_4), perchloric acid ($HClO_4$), hydrogen peroxide (H_2O_2), and Immunoglobulin G antigen (IgG) were obtained from Sigma-Aldrich (St. Louis, MO, USA). Amyloid β (1–42), the human peptide was purchased from GenScript. The preparation of Aβ oligomers was based on previous work (Tsukakoshi et al., 2012). The preparation process is denoted in the electronic supporting material. The amino-terminal aptamer probe was purchased from the Nzytech company and its sequence was:

NH_2-$(CH_2)_6$GCCTGTGGTGTTGGGGCGGGTGCG (Tsukakoshi et al., 2012).

2.2. Apparatus

Scanning electron microscopy (SEM) was performed with an FEI Quanta 600. Infrared spectra were obtained using a JASCO FT/IR-680 Plus Fourier transform infrared (FTIR) spectrometer. UV–Visible (Uv–Vis) absorption spectrum was performed on a PerkinElmer UV–Vis spectrophotometer. Raman scattering was performed on a Renishaw's inVia Raman spectrometer using 514 nm laser source. Energy Dispersive X-Ray (EDX) spectra were obtained using Oxford Instruments. The interferometric reflectance spectra were recorded using an AvaSpec-ULS3648 fiber optic spectrometer. The measurement set-up cell is shown in Fig.S1.

2.3. Fabrication of NAA

NAA was prepared based on the previous method (Marsal et al., 2009; Santos et al. 2011a, 2011b). Briefly, Aluminium (Al) disc of 15 mm diameter was first cleaned in ethanol and water (50: 50) under ultra-sonication for 5 min and then in acetone for 5 min to remove any pollution on the surface of Al. To electro-polish of Al disc, the freshly cleaned Al disc was attached to the electrochemical cell. After that, Al disc was anodized at 20 V in an ethanol solution containing $HClO_4$ (25%) for 10 min. Subsequently, Al disc was washed several times and dried under compressed airflow to remove all residual $HClO_4$. The first step anodization was then carried out in 0.3 M Ox at 40 V and 5 °C for 20 h. The Al disc was then rinsed by water and ethanol for 5 min and dried under compressed air flow. Afterward, Al disc was dissolved by wet chemical etching in a solution containing 0.4 M H_3PO_4 and 0.2 M H_2CrO_4 for 3 h at 70 °C. The Al disc was then rinsed by water and ethanol for 10 min and dried under compressed air flow. Afterward, the second step anodization was performed under the same conditions as first anodization and it was done until a total charge of 20 C was passed to obtain a layer of 5 μm thickness. The pore widening was done by wet chemical etching by immersing in 5% H_3PO_4 for 20 min.

2.4. Fabrication of aptasensor

To provide high fidelity interferometric reflectance of NAA, the surface of NAA was first coated with 10 nm thick gold layer under vacuum at 30 mA for 1 min using an EMITech K575X sputter coater. After that, NAA was immersed into a 3.0 M H_2O_2 solution (T = 70 °C) for 1 h to removes any organic contaminants from the surface and actives the native hydroxyl groups of NAA. Then, NAA was washed with water for 30 s and dried under nitrogen gas flow. Subsequently, NAA was immersed into 1% 3-APES solution (ethanol/H_2O 3:1) for 30 min under nitrogen gas atmosphere to introduce amine groups inside of the pore of NAA. NAA-NH_2 was then rinsed with water for 1 min and dried under nitrogen gas flow. After that, the NAA-NH_2 was dried under a nitrogen atmosphere at 100 °C for 2 h. Subsequently, the NAA-NH_2 was immersed in a 2.5% GLA in PB and stirred for 1 h. NAA−NH−GLA was then rinsed with water and dried under nitrogen gas flow. The amino aptamer solution (20 mL, 1 mM, 0.1 M PB of pH 7.4) was dropped on the NAA−NH−GLA and incubated for 12 h at room temperature. During this time, the amino-terminal aptamers were attached to the aldehyde groups of GLA. After that, NAA−NH−GLA−NH−aptamer was rinsed thoroughly with double distilled water to wash away the loosely adsorbed aptamers. NAA−NH−GLA−NH−aptamer is immersed in the PB (pH 7.4) containing 50 μM of MB for 30 min at room temperature to immobilize the MB into the intermolecular G-quadruplex structures. Then, the BSA solution (0.25%, 0.1 M PB of pH 7.4, dissolved on a rotator for 30 min) was dropped on the NAA to decrease the non-specific binding for 30 min. Finally, the fabricated aptasensor (NAA−NH−GLA−NH−aptamer/MB) was rinsed thoroughly with water to wash away the loosely adsorbed BSA. The apasensor was stored at 4 °C when not in use. The schematic illustration of the aptasensor fabrication employed is shown in Fig. 1.

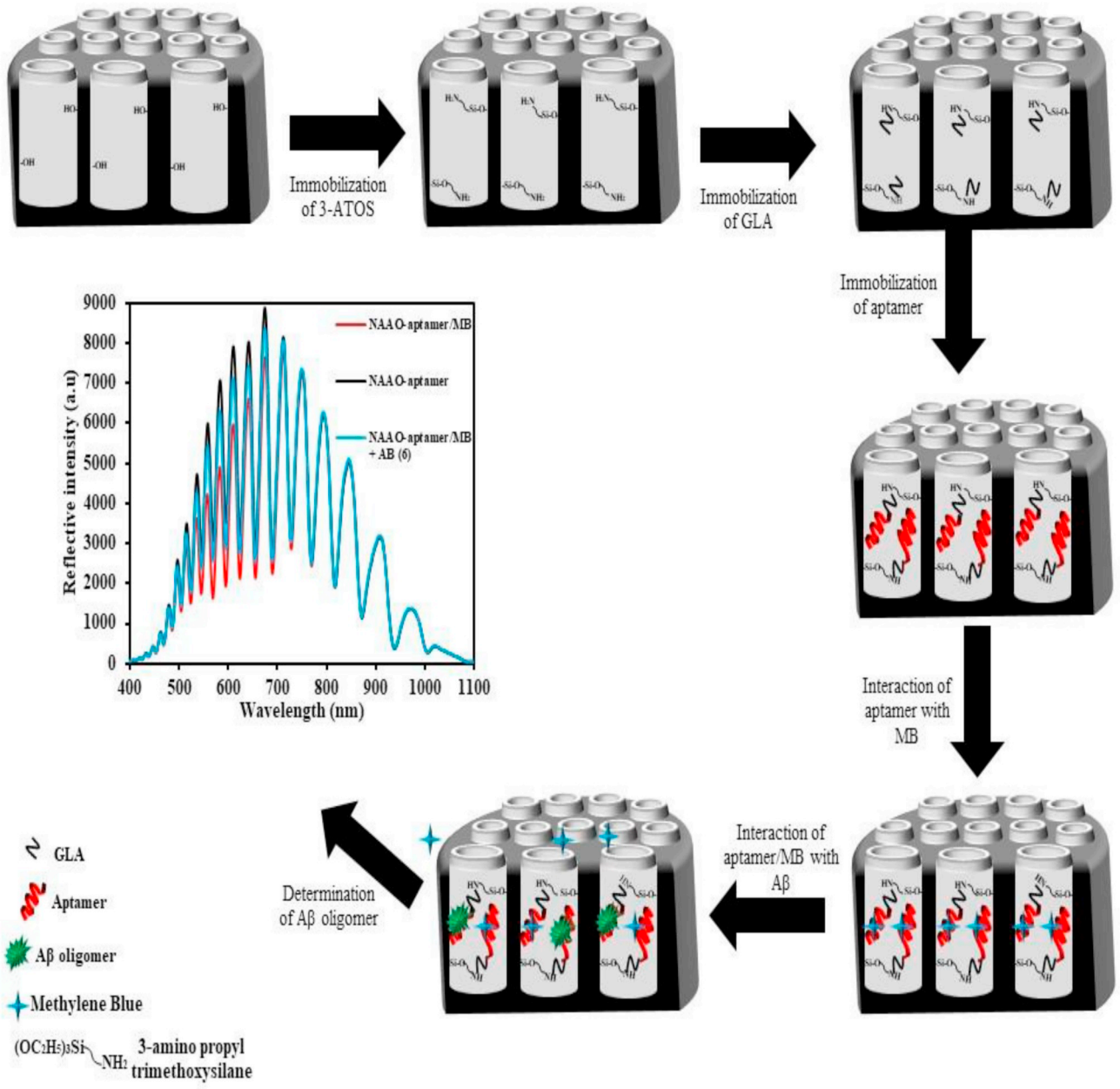

Fig. 1. The schematic illustration for the fabrication of IRS based aptasensor.

2.5. The sensing process of Aβ oligomers

The aptasensor was transferred to a flow cell set-up and injected the different concentrations of Aβ oligomers. Under the optimized conditions, the change in the peak area versus the logarithm of the concentration of Aβ oligomers was recorded.

3. Results and discussion

3.1. Surface characterization of NAA

Top view (A) and cross-section (B) SEM images of NAA are shown in Fig. 2. As can be seen, NAA has the highly hexagonal-ordered nanoporous structure. The average pore size of NAA was approximately 54 nm.

FTIR spectroscopy was employed to characterize the structure of the prepared NAA−NH−GLA−NH−aptamer, and NAA−NH−GLA−NH−aptamer/MB (Fig. 3A). Fig. 3A(a) shows a typical FTIR spectrum recorded for NAA−NH−GLA−NH−aptamer in which absorption bands at 1159 cm^{-1} and 955 cm^{-1} due to the Al−O−H and Al−O modes of boehmite are clearly seen (Liu et al., 2012). The other characteristic absorption bands of NAA−NH−GLA−NH−aptamer such as a band at 2919 cm^{-1} due to the $-CH_2$, $-CH_3$ stretching, a band at 2372 cm^{-1} due to the $-NH_2$, a band at 1210 cm^{-1} due to the –P═O stretching (as the aptamer backbone), a band at 1580 cm^{-1} due to the R−CONH−R' (N−H band, secondary amide), a band at 1426 cm^{-1} due to the −CN stretching band (Ede et al., 2014) of the aptamer chain and a band at 823 cm^{-1} due to the vibration of Si−O−Si of 3-APES (White and Tripp, 2000) are clearly seen. All these bands provide that the aptamer was successfully immobilized on NAA. After the incubation of MB with aptamer on NAA-aptamer, two new peaks are observed at 734 cm^{-1} due to the C−S−C and at 823 cm^{-1} due to the C−H (in the aromatic structure) (Agarwala et al., 1967) stretching from the MB, indicating the adoptions of MB on the aptasensor (Fig. 3A(b)). Raman spectroscopy is one of the most widely used techniques for the characterization of the adsorbed photo-probes like MB. Fig. 3B shows a typical Raman

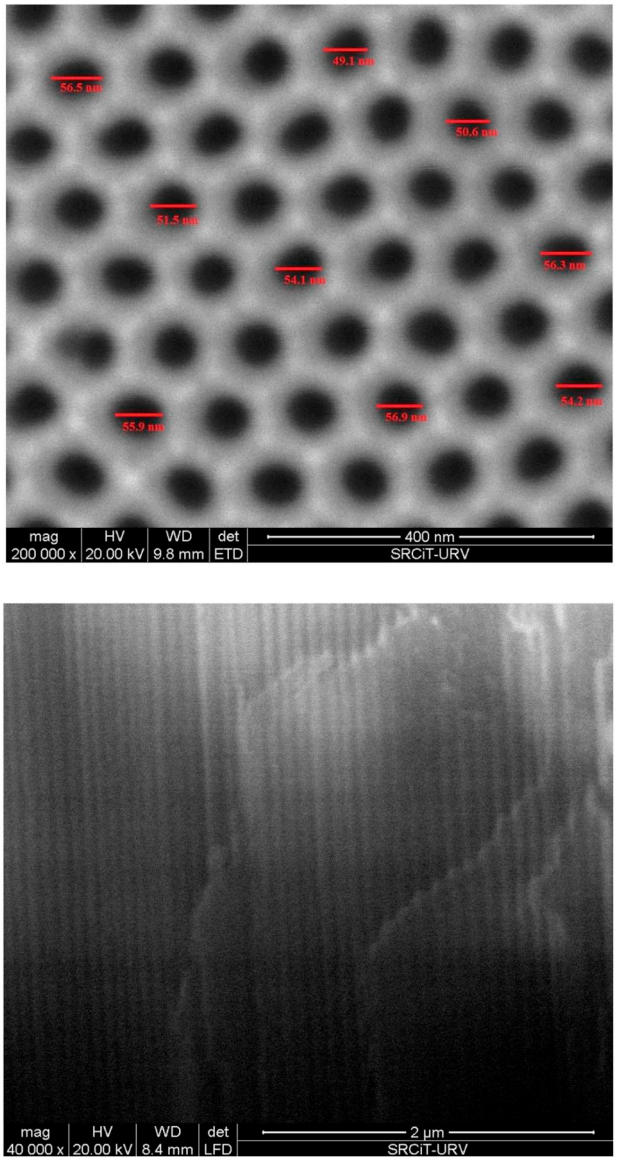

Fig. 2. (A) Top view and (B) cross-section SEM images of NAA.

spectrum recorded for NAA—NH—GLA—NH—aptamer (a) and NAA—NH—GLA—NH—aptamer/MB (b). As can be seen, a band at 1090 cm^{-1} due to –P═O bond as the aptamer backbone (Kuhar et al., 2018) is seen in Fig. 3B(a). The appearance of this peak indicates that aptamer was immobilized on NAA, successfully. After the immobilization of MB into the intermolecular G-quadruplex structures on NAA—NH—GLA—NH—aptamer (Fig. 3B (b)), a strong band was observed at 1620 cm^{-1} due to C—C ring mode of MB (Li et al., 2016). The results are reliable with the FTIR results.

Fig. 3C displays EDX spectra of NAA—NH—GLA—NH—aptamer (a) and NAA—NH—GLA—NH—aptamer/MB (b). The peaks were obtained at 0.3 keV due to the carbon element, 0.5 keV due to Oxygen element, 1.4 keV due to Aluminium element, 1.75 keV due to Silicon, 2 keV due to Phosphorus element, and 2.3 keV due to Sulphur element. All results demonstrate that aptamer and MB were immobilized on NAA.

3.2. Optical characterization of sensing interface

Fig. 4A shows the typical the interference spectra of NAA—NH—⊜ GLA—NH—aptamer (a), NAA—NH—GLA—NH—aptamer/MB (b), and NAA—NH—GLA—NH—aptamer/MB after the interaction with 6.0 µg × mL^{-1} of Aβ oligomers (c). As can be seen, after the interaction of MB with the immobilized aptamer, the signal intensity between 400 nm and 725 nm dramatically decreased because of the generation of the MB/G-quadruplex complex in the site the NAA. On the other hand, the UV–Vis spectrum of MB solution demonstrated that the MB solution adsorbs the light between 550 nm and 725 nm but it is transparent in the higher wavelength (Fig. 4B). Also, the IRS of NAA in the absence (a) and presence of MB (b) (500 µM, PB 0.1 M, pH 7.4) shows the intensity decrease until 725 nm (Fig. 4C). The reasonable explanation for the difference between the interference spectrums of the NAA—NH—⊜ GLA—NH—aptamer (Fig. 4A (a)) and the NAA—NH—GLA—NH—aptamer/MB (Fig. 4A (b)) is that the immobilized MB into the G-quadruplex structures adsorbed the light in this wavelength range and therefore the intensity of the reflected light to the detector (charge-coupled device (CCD)) decreased. But after the incubation of Aβ oligomers with aptamer in the NAA—NH—GLA—NH—aptamer/MB, the MB/G-quadruplex complex broke and MB desorbed into the solution and then washed away by PB (0.1 M, pH 7.4). Therefore, the intensity of the reflected light to the CCD detector increased (Fig. 4A(c)).

Fig. 5A shows the IRS of NAA—NH—GLA—NH—aptamer before (a) and after (b) the immobilization of MB. The subtraction of the spectrum of 5A(a) from 5A(b) clearly demonstrated that MB in the MB/G-quadruplex complex adsorbed the light and therefore the reflected light to CCD detector decreased (Fig. 5A(c)).

Fig. 5B also shows the IRS of NAA—NH—GLA—NH—aptamer/MB before (a) and after (b) the incubation with Aβ oligomers (6.0 µg × mL^{-1}). The subtraction of spectrum of 5B(a) from 5B(b) demonstrated that Aβ oligomers broke the MB/G-quadruplex complex and therefore the reflected light to CCD detector increased (Fig. 5A(c). It can be seen that the Δpeak area can be used as a signal to recognize the changes in the optical property of aptasensor.

3.3. Optimization of effective parameters on the response of aptasensor

The influence of the pH solution and incubation time of Aβ oligomers (6.0 µg × mL^{-1}) in the aptasensor were studied (Fig. S2). As shown in Fig. S2A, the response of aptasensor increased rapidly with increasing incubation time up to 2 h, and remained unchanged at longer incubation times, indicating the formation of Aβ oligomers/aptamer has reached to the saturation level. Also, Fig. S2B shows the influence of pH value on the response of aptasensor to Aβ oligomers. As shown in this figure, the responses of aptasensor increased by increasing pH and reached to the maximum intensity at pH 7.4 and then decreased after that. The reasonable explanation is that the nucleotide bases in the aptamer were protonated and then the MB/G-quadruplex complex broke in the acidic solution. In addition, the functional groups of Aβ oligomers also protonated in the acidic solution. The protonated Aβ oligomers could not interact with the aptamer. Another hand, the alkaline solutions can inactivate the biomolecules such as aptamers and oligomers and prevent the formation of the aptamer-Aβ oligomers complex.

Therefore, the accumulation time of 2 h and solutions with a pH 7.4 have been chosen as the optimum condition for the determination of Aβ oligomers throughout this work. These parameters were optimized at 37 °C.

3.4. Determination of Aβ oligomers

Under the optimized conditions, the concentration of Aβ oligomers was detected (Fig. 6). As shown in Fig. 6A, after the incubation of Aβ oligomers with the immobilized aptamer in the NAA—NH—GLA—NH—aptamer/MB, the MB/G-quadruplex complex broke and MB washed away by the flow of PB (0.1 M, pH 7.4). Hence, the Δpeak area increased with increasing Aβ oligomers concentration ($C_{Aβ}$). The Δpeak area exhibited a good linear response to the logarithm of the concentration Aβ oligomers in the linear range from 0.5 to 50.0 µg × mL^{-1}

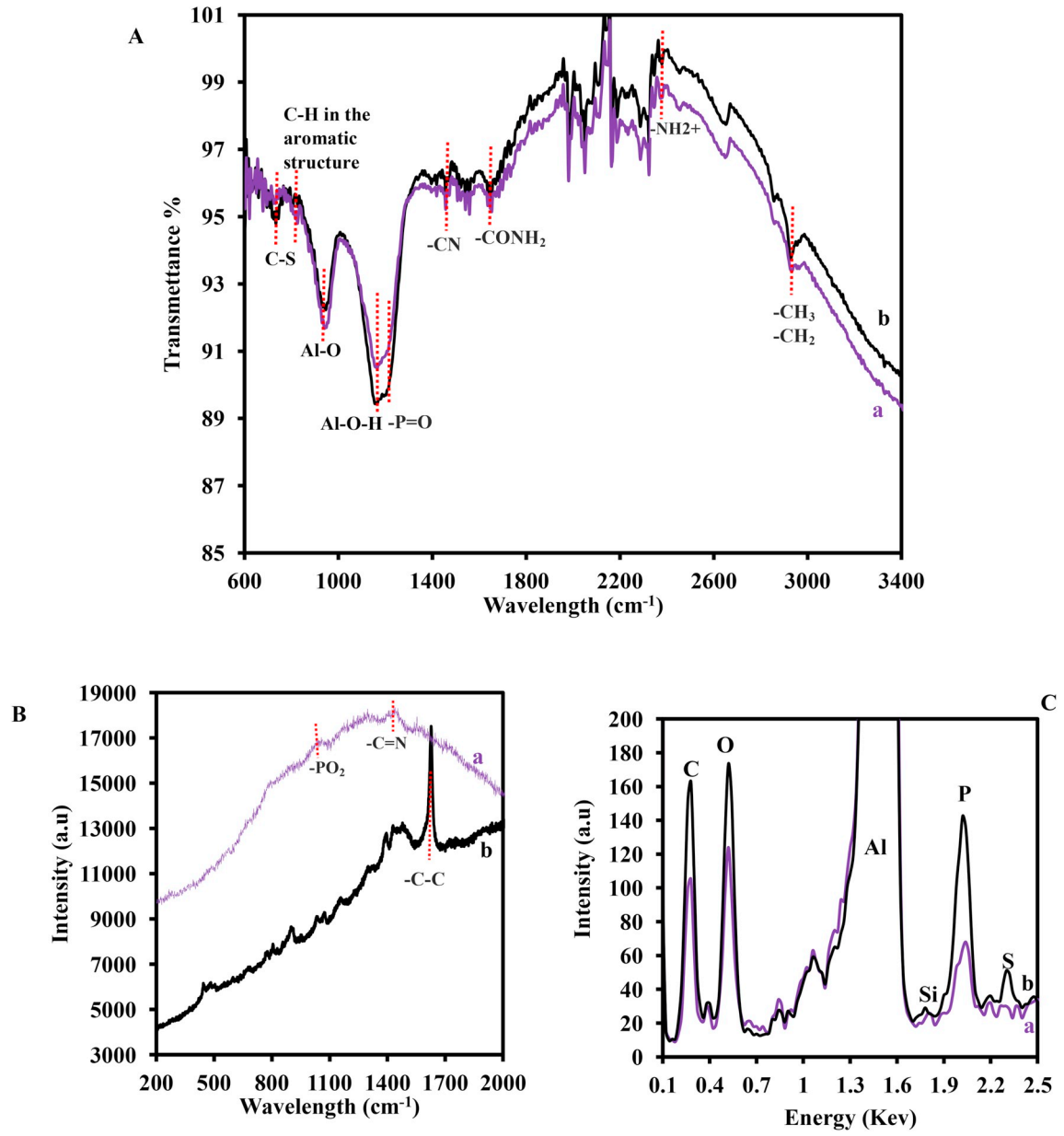

Fig. 3. (A) FTIR, (B) Raman and (C) EDX spectra of (a) NAA—NH—GLA—NH—aptamer, and (b) NAA—NH—GLA—NH—aptamer/MB.

(Fig. 6B). The linear regression equation of the calibration curve is expressed as Δpeak area = 134468 Log $C_{Aβ}$ (μg × mL^{-1}) +117107 with a correlation coefficient of 0.982 (n = 9) (Fig. 6B). The error bars represent the calculated standard deviation for the four measurements. The limit of detection (LOD) is 0.02 μg × mL^{-1} (at 3σ/S), where σ is the standard deviation of the blank measurements and S is the slope. The obtained LOD was lower than the previous optical biosensors (Baliyan et al., 2016; Carrasquilla et al., 2011; DeLisa et al., 2000; Rajeev et al., 2018; Shevchenko et al., 2011).

The change in the effective optical thickness (ΔEOT) of interferometric reflectance based biosensor before and after interaction with the target is a common method for the determination of targets (Chhasatia et al., 2017; Lin et al., 1997). Fig. S3 shows the ΔEOT versus the Aβ oligomers concentration. As shown in this figure, not only the slope of the plot is so lower than Fig. 6B but also a linear range of plot is narrow. Therefore, using the Δpeak area as a sensing parameter is better than ΔEOT.

Also, the amount of change in the EOT for 0.60 μg × mL^{-1} Aβ oligomers concentration in the aptamer/MB based sensor is 60 times higher than the aptamer based sensor (Fig. S4). The reasonable reason is that the interaction of Aβ oligomers with the proposed aptasensor occurred through two steps: First, the aptamer/MB complex should be broken and adsorbed MB should be desorbed from the immobilized aptamer probes and then these free aptamer probes can interact with Aβ oligomers concentration. Therefore, the EOT of NAA will be changed in each step. The mechanism of incubation of Aβ oligomers with NAA—NH—GLA—NH—aptamer/MB is denoted in below schematically:

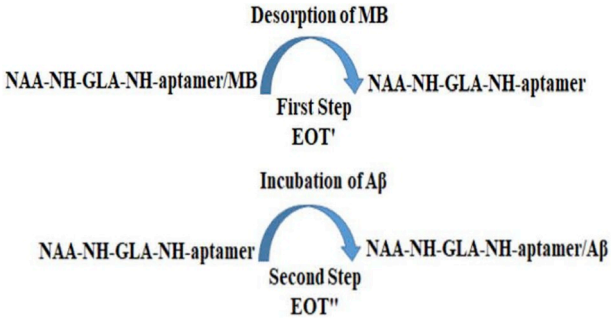

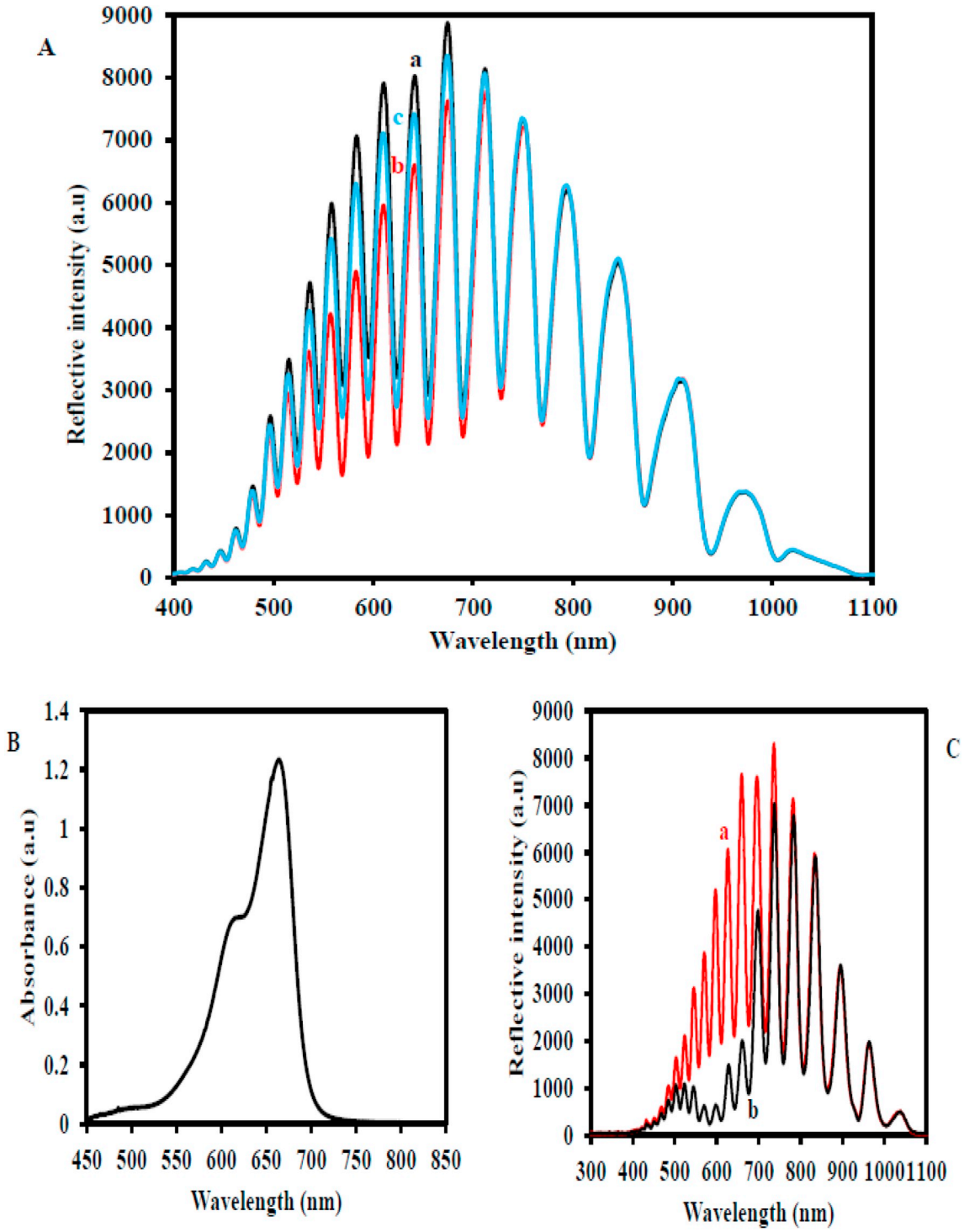

Fig. 4. (A) The IRS of (a) NAA−NH−GLA−NH−aptamer, (b) NAA−NH−GLA−NH−aptamer/MB, and (c) NAA−NH−GLA−NH−aptamer/MB after the interaction with 6.0 μg × mL^{-1} of Aβ oligomers. (B) UV–vis absorption spectra of MB. (C) IR spectra of NAA in PB (0.1 M, pH 7.4) in absence (a) and presence of MB (0.1 mM) (b).

As shown in this scheme, this extra desorption of MB in the first step did not happen in the incubation of Aβ oligomers with the NAA−NH−GLA−NH−aptamer.

Therefore, the study of Δpeak area versus the concentration of target in the aptamer/MB based aptasensor is a new strategy to fabricate the high sensitive aptasensor in the IRS based aptasensor.

Also, Fig. S5A and B show the Langmuir (A) and Freundlich (B) binding isotherm models for Aβ oligomers on the NAA−NH−GLA−NH−aptamer/MB aptasensor. As can be seen, the experimental data were best fitted by the Langmuir binding isotherm model. Therefore, the binding of Aβ oligomers to aptamer in the proposed aptasensor followed a monolayer adsorption mechanism.

The target/aptamer dissociation constant (K_d) that is the reverse of Langmuir constant (K_L) was 2.66 μg × mL^{-1}. The constant parameters and correlation coefficient for these binding isotherm models and the related equations are denoted in the inset of Fig. S5.

The effect interfering BSA, and IgG was also studied on the determination of oligomers (Fig. S6A). As shown in this figure, the

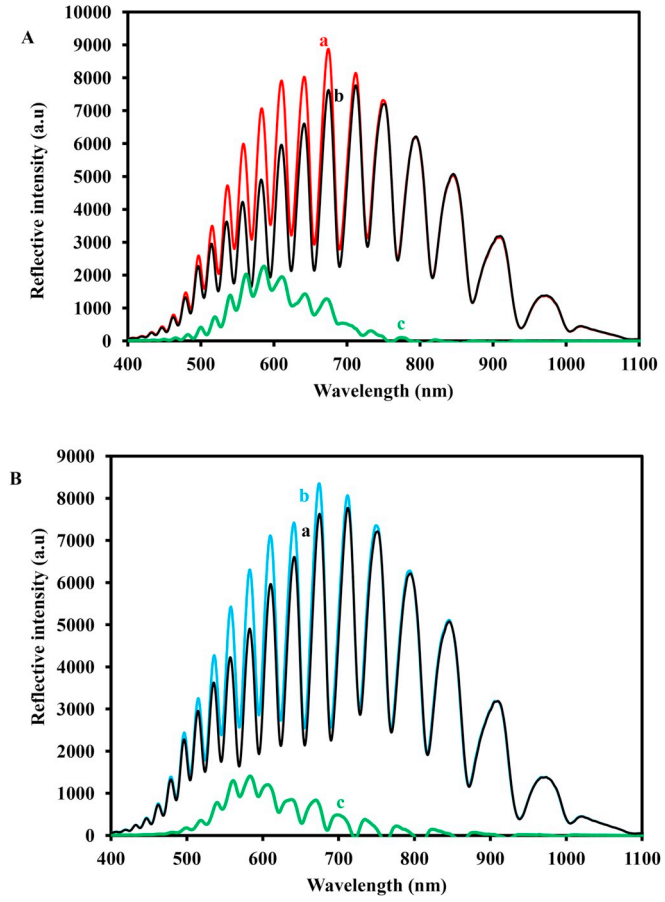

Fig. 5. (A) The IRS of (a) NAA−NH−GLA−NH−aptamer, (b) NAA−NH−GLA−NH−aptamer/MB and (c) the difference between these two interference spectra in PB (0.1 M, pH 7.4). (B) The IRS of NAA−NH−GLA−NH−aptamer/MB in before (a) and after (b) the incubation with Aβ oligomer (6.0 μg × mL^{-1}), and (c) the difference between these two interference spectra in PB (0.1 M, pH 7.4).

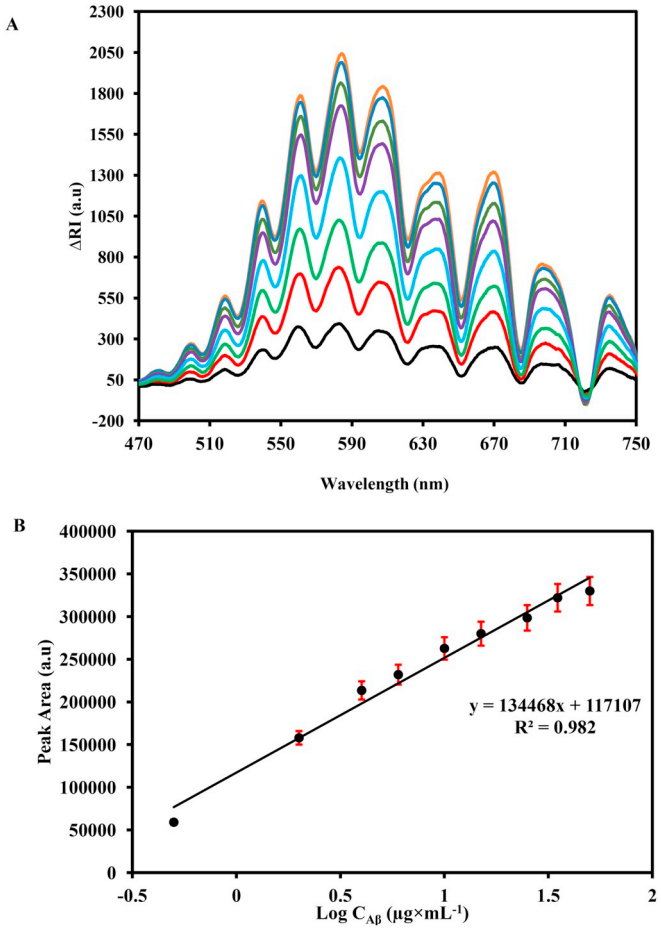

Fig. 6. (A) The response of aptasensor at the optimum conditions for different amounts of Aβ oligomers (0.5, 2, 4, 6, 10, 15, 25, 35, and 50 μg × mL^{-1}). (B) The calibration plot of aptasensor toward Aβ oligomers. Each value is presented as mean ± SD, n = 4.

NAA−NH−GLA−NH−aptamer/MB has a high selectivity to Aβ oligomers. The concentrations of the interfering substances were 5.0 times of Aβ oligomers (6.0 μg × mL^{-1}). The relative standard deviation (RSD) was also found to be 7.8% after 14 days (Fig. S6B). Aptasensors' reproducibility was also evaluated for determinations of 6.0 μg × mL^{-1} of Aβ oligomers with four different NAA−NH−GLA−NH−aptamer/MB. The RSD was calculated to be 9.2% which indicated that the proposed aptasensor had good reproducibility. Therefore, the analytical performances of the NAA−NH−GLA−NH−aptamer/MB are comparable with other biosensors (Mariani et al., 2016; Pol et al., 2019; Rajeev et al., 2018).

In this work, we achieved two main aim: First, improving the sensitivity of aptasensor based on IRS and second, put an end to use the time-consuming method to analysis the EOT as a signal.

4. Conclusions

A novel strategy for fabrication of aptasensor based on IRS has been developed. The guanine-rich aptamers and MB were used as the molecular recognition element and photo-probe, respectively to detect Aβ oligomers as a model of the target. The MB/G-quadruplex complex plays the main role in the fabrication of the proposed aptasensor. Upon addition of Aβ oligomers, the MB/G-quadruplex complex broke and MB desorbed into the solution and consequently, the intensity of the reflected light to CCD detector increased. According to the results obtained in this study, we believe that this kind of the aptamer/photo-probe will open the new chapter in the field of the aptasensor based on IRS. However, the proposed aptasensor suffers from a major limitation. In comparison with the immunosensors can detect Aβ in its peptide form (Gonçalves et al., 2016), the proposed apatsensor only can be used for the sensing of Aβ in its oligomers form. So, a pre-treatment process should be done on the biological samples containing Aβ peptide to change it to oligomer form.

CRediT authorship contribution statement

Mahmoud Amouzadeh Tabrizi: Methodology, Formal analysis, Investigation, Writing - original draft. **Josep Ferré-Borrull:** Formal analysis. **Lluis F. Marsal:** Supervision, Writing - review & editing, Resources, Project administration, Funding acquisition.

Acknowledgments

This research was partially supported by the Spanish Ministerio de Ciencia, Innovación y Universidades RTI2018-094040-B-I00 (MICINN/FERDER), by the Agency for Management of University and Research Grants (AGAUR) ref. 2017-SGR-1527, by the Catalan Institution for Research and Advanced Studies (ICREA) under the ICREA Academia Award and by the Martí-Franquès II postdoctoral programme under grant number 2017PMF-POST2-7. The project leading to these results has also received funding from “la Caixa” Foundation under the agreement LCF/PR/PR17/11120023. The authors would like to thank Mrs. Mercè Moncusí Mercadé, Mrs. Mariana Stefanova Stankova, and

Mrs. Debora Cano Acedo for their kindly technical assistance with the SEM, Raman and FTIR characterization process.

Appendix A. Supplementary data

Supplementary data related to this article can be found at https://doi.org/10.1016/j.bios.2019.04.050.

References

Agarwala, U., Narayan, V.A., Dikshit, S.K., 1967. Can. J. Chem. 45, 1057–1062.
Amouzadeh Tabrizi, M., Shamsipur, M., Saber, R., Sarkar, S., 2018. Biosens. Bioelectron. 110, 141–146.
Amouzadeh Tabrizi, M., Shamsipur, M., 2015. Biosens. Bioelectron. 69, 100–105.
Baliyan, A., Sital, S., Tiwari, U., Gupta, R., Sharma, E.K., 2016. Long period fiber grating based sensor for the detection of triacylglycerides. Biosens. Bioelectron. 79, 693–700.
Bandodkar, A.J., Jia, W., Yardımcı, C., Wang, X., Ramirez, J., Wang, J., 2015. Anal. Chem. 87, 394–398.
Burge, S., Parkinson, G.N., Hazel, P., Todd, A.K., Neidle, S., 2006. Nucleic Acids Res. 34 (19), 5402–5415.
Cao, Q., Li, Y., Freisinger, E., Qin, P.Z., Sigel, R.K.O., Mao, Z.-W., 2017. Inorg. Chem. Front. 4, 10–32.
Carrasquilla, C., Xiao, Y., Xu, C.Q., Li, Y., Brennan, J.D., 2011. Anal. Chim. 83, 7984–7991.
Chiavaioli, F., Gouveia, C.A.J., Jorge, P.A.S., Baldini, F., 2017. Biosensors 7, 1–29.
Chhasatia, R., Sweetman, M.J., Harding, F.J., Waibel, M., Kay, T., Thomas, H., Loudovaris, T., Voelcker, N.H., 2017. Biosens. Bioelectron. 91, 515–522.
Citron, M., Diehl, T.S., Gordon, G., Biere, A.L., Seubert, P., Selkoe, D.J., 1996. Proc. Natl. Acad. Sci. U.S.A. 93, 13170–13175.
DeLisa, M.P., Zhang, Z., Shiloach, M., Pilevar, S., Davis, C.C., Sirkis, J.S., Bentley, W.E., 2000. Biosensor. Anal. Chim. 72, 2895–2900.
Deng, C., Liu, H., Zhang, M., Deng, H., Lei, C., Shen, L., Jiao, B., Tu, Q., Jin, Y., Xiang, L., Deng, W., Xie, Y., Xiang, J., 2018. Anal. Chim. 90, 1710–1717.
Ede, S.R., Ramadoss, A., Anantharaj, S., Nithiyanantham, U., Kundu, S., 2014. Phys. Chem. Chem. Phys. 16, 21846–21859.
Fan, D., Guo, C., Ma, H., Zhao, D., Li, Y., Wu, D., Wei, Q., 2016. Biosens. Bioelectron. 75, 116–122.
Ferré-Borrull, J., Pallarès, J., Macías, G., Marsal, L.F., 2014. Materials 7, 5225–5253.
Galán, T., Prieto-Simón, B., Alvira, M., Eritja, R., Götz, G., Bäuerle, P., Samitier, J., 2015. Biosens. Bioelectron. 74, 751–756.
Gonçalves, J.M., Lima, L.R., Moraes, M.L., Ribeiro, S.J.L., 2016. Mater. Sci. Eng. C 68, 338–342.
Heeres, J.T., Hergenrother, P.J., 2011. Chem. Soc. Rev. 40, 4398–4410. 2017. (eurekalert). https://www.eurekalert.org/pub_releases/2017-08/tl-tlg080117.php.
Jarczewska, M., Rębiś, J., Górski, Ł., Malinowska, E., 2018. Talanta 189, 45–54.
Ke, H., Sha, H., Wang, Y., Guo, W., Zhang, X., Wang, Z., Huang, C., Jia, N., 2018. Biosens. Bioelectron. 100, 266–273.
Kolpashchikov, D.M., 2005. J. Am. Chem. Soc. 127, 12442–12443.
Kuhar, N., Sil, S., Verma, T., Umapathy, S., 2018. RSC Adv. 8, 25888–25908.
Kumeria, T., Santos, A., Rahman, M.M., Ferré-Borrull, J., Marsal, L.F., Losic, D., 2014. ACS Photonics 1, 1298–1306.
Li, C., Huang, Y., Lai, K., Rasco, B.A., Fan, Y., 2016. Food Control 65, 99–105.
Lin, V.S.Y., Motesharei, K., Dancil, K.-P.S., Sailor, M.J., Ghadiri, M.R., 1997. Science 278, 840–843.
Liu, L., Xia, N., Zhang, J., Mao, W., Wu, Y., Ge, X., 2015. Anal Methods 7, 8727–8732.
Liu, C., Shih, K., Gao, Y., Li, F., Wei, L., 2012. J. Soils Sediments 12, 724–733.
Lublin, A.L., Gandy, S., 2010. 77. Mt Sinai J Med, New York, pp. 43–49.
Malmir, K., Habibiyan, H., Ghafoorifard, H., 2016. Optic Commun. 365, 150–156.
Marazuela, M., Moreno-Bondi, M., 2002. Anal. Bioanal. Chem. 372, 664–682.
Mariani, S., Pino, L., Strambini, L.M., Tedeschi, L., Barillaro, G., 2016. ACS Sens. 1, 1471–1479.
Marsal, L.F., Vojkuvka, L., Formentin, P., Pallarés, J., Ferré-Borrull, J., 2009. Opt. Mater. 31, 860–864.
Mc Keague, M., Velu, R., Hill, K., Bardóczy, V., Mészáros, T., DeRosa, M.C., 2014. Toxins 6, 2435–2452.
Nemati, M., Santos, A., Losic, D., 2018. Sensors 18, 470–488.
Miloševic, Maja D., Mihovil Logar, M., Vesna Poharc-Logar, A., Ljiljana Jakšic, N., 2013. Int J Spectrosc 2013, 1–6.
Pol, L., Eckstein, C., Acosta, L.K., Xifre-Perez, E., Ferre-Borrull, J., Marsal, L.F., 2019. Nanomaterials 9, 1–12.
Rajeev, G., Xifre-Perez, E., Prieto Simon, B., Cowin, A.J., Marsal, L.F., Voelcker, N.H., 2018. Sensor. Actuator. B Chem. 257, 116–123.
Rushworth, J.V., Ahmed, A., Griffiths, H.H., Pollock, N.M., Hooper, N.M., Millner, P.A., 2014. Biosens. Bioelectron. 56, 83–90.
Salvadores, N., Shahnawaz, M., Scarpini, E., Tagliavini, F., Soto, C., 2014. Cell Rep. 7, 261–268.
Santos, A., Ferré-Borrull, J., Pallarès, J., Marsal, L.F., 2011a. Phys. Status Solidi 208, 668–674.
Santos, A., Formentín, P., Pallarès, J., Ferré-Borrull, J., Marsal, L.F., 2011b. J. ElectroAnal. Chim. 655, 73–78.
Shamsipur, M., Farzin, L., Amouzadeh Tabrizi, M., Molaabasi, F., 2015. Biosens. Bioelectron. 74, 369–375.
Shevchenko, Y., Francis, T.J., Blair, D.A.D., Walsh, R., DeRosa, M.C., Albert, J., 2011. Anal. Chim. 83, 7027–7034.
Song, G., Ren, J., 2010. Chem. Commun. 46, 7283–7294.
Song, X., Fu, B., Lan, Y., Chen, Y., Wei, Y., Dong, C., 2018. Spectrochim. Acta Mol. Biomol. Spectrosc. 204, 301–307.
Stavra, E., Petrou, P.S., Koukouvinos, G., Kiritsis, C., Pirmettis, I., Papadopoulos, M., Goustouridis, D., Economou, A., Misiakos, K., Raptis, I., Kakabakos, S.E., 2018. J. Hazard Mater. 359, 67–75.
Tew, D.J., Bottomley, S.P., Smith, D.P., Ciccotosto, G.D., Babon, J., Hinds, M.G., Masters, C.L., Cappai, R., Barnham, K.J., 2008. Biophys. J. 94, 2752–2766.
Tsukakoshi, K., Abe, K., Sode, K., Ikebukuro, K., 2012. Anal. Chim. 84, 5542–5547.
Veloso, A.J., Chow, A.M., Ganesh, H.V.S., Li, N., Dhar, D., Wu, D.C.H., Mikhaylichenko, S., Brown, I.R., Kerman, K., 2014. Anal. Chim. 86, 4901–4909.
Vojkuvka, L., Marsal, L.F., Ferré-Borrull, J., Formentin, P., Pallarés, J., 2008. Superlattice. Microst. 44, 577–582.
Wang, J., Meng, W., Zheng, X., Liu, S., Li, G., 2009. Biosens. Bioelectron. 24, 1598–1602.
White, L.D., Tripp, C.P., 2000. J. Colloid Interface Sci. 232, 400–407.
Wu, Y., Sefah, K., Liu, H., Wang, R., Tan, W., 2010. Proc. Natl. Acad. Sci. U.S.A. 107, 5.
Yi, X., Feng, C., Hu, S., Li, H., Wang, J., 2016. Analyst 141, 331–336.
Zarei, S.S., Soleimanian-Zad, S., Ensafi, A.A., 2018. Microchim. Acta 185, 538–547.
Zhang, F.-T., Nie, J., Zhang, D.-W., Chen, J.-T., Zhou, Y.-L., Zhang, X.-X., 2014. Anal. Chim. 86, 9489–9495.
Zhang, X., Li, S., Jin, X., Zhang, S., 2011. Chem. Commun. 47, 4929–4931.
Zhou, Y., Li, C., Li, X., Zhu, X., Ye, B., Xu, M., 2018. Anal Methods 10, 4430–4437.
Zhou, Y., Zhang, H., Liu, L., Li, C., Chang, Z., Zhu, X., Ye, B., Xu, M., 2016. Sci. Rep. 6, 35186.